Journal of Applied Physics

RESEARCH ARTICLE | JUNE 10 2025

Accuracy of joint refractive index and phonon velocity estimation using Brillouin light backscattering in the platelet geometry

Fehima Ugarak ; Alexis Mosset ; Vincent Laude

J. Appl. Phys. 137, 223103 (2025)
https://doi.org/10.1063/5.0274234

Journal of Applied Physics METHOD pubs.aip.org/aip/jap

Accuracy of joint refractive index and phonon velocity estimation using Brillouin light backscattering in the platelet geometry

Cite as: J. Appl. Phys. **137**, 223103 (2025); doi: 10.1063/5.0274234
Submitted: 4 April 2025 · Accepted: 25 May 2025 ·
Published Online: 10 June 2025

Fehima Ugarak, Alexis Mosset, and Vincent Laude[a)]

AFFILIATIONS

Université Marie et Louis Pasteur, CNRS, Institut FEMTO-ST, 15B avenue des Montboucons, 25030 Besançon, France

[a)]**Author to whom correspondence should be addressed:** vincent.laude@femto-st.fr

ABSTRACT

Brillouin light backscattering from isotropic platelet samples involves the contribution of two phase-matched longitudinal acoustic phonons. A primary, stronger, signal is provided by the usual condition of a phonon wavevector collinear to and twice as large as the incident photon wavevector inside the medium. After reflection of incident light on the backside of the platelet, another bulk phonon propagating along the platelet axis contributes a secondary, weaker, signal that is independent of the index of refraction but dependent on the angle of incidence. Combining contributions from both phonons, the refractive index and the acoustic phonon velocity can be estimated jointly and precisely in the backscattering geometry from experimental data. Experiments with poly(methyl methacrylate), fused silica, and soda-lime glass platelets are used to assess the accuracy of the estimation. It is argued that the secondary Brillouin signal dictates the estimation of velocity whereas the primary Brillouin signal dictates the estimation of the index of refraction.

I. INTRODUCTION

Brillouin scattering or inelastic light scattering from acoustic phonons of thermal origin is widely adopted for the characterization of the elastic properties of materials.[1–3] The Brillouin frequency shift ω is proportional to the phonon velocity v and to the phonon wavenumber q, as per the dispersion relation $\omega = vq$. The phonon wavenumber is imposed by momentum conservation in the photon-phonon interaction, or by phase-matching in a classical wave picture, and thus depends on the chosen scattering geometry,[4,5] as Fig. 1 depicts. The backscattering configuration [Fig. 1(a)] offers a relatively large interaction volume, enabling higher temporal resolution and faster acquisition of Brillouin spectra compared to other commonly used scattering geometries.[6] It also demands easier alignment and provides larger Brillouin frequency shifts independent of the angle of incidence for isotropic materials, since

$$\omega_1 = q_1 v = 2knv, \tag{1}$$

with $k = 2\pi/\lambda$ and λ the optical wavelength in a vacuum, and with n the index of refraction. Using the backscattering geometry enables the precise determination of the Brillouin frequency and hence of the product nv. Estimating velocities is however often the main goal, since the elastic constants depend directly on them, and the index of refraction has to be either assumed or determined independently, e.g., by ellipsometry. When the second option is not available, the first option can be inconvenient since a systematic bias is introduced in the acoustic velocity estimation if the value selected for the index of refraction is incorrect or imprecise.

The 90°-scattering geometry [Fig. 1(b)] requires a special parallelepipedic sample shape and imposes

$$\omega_2 = q_2 v = \sqrt{2}knv. \tag{2}$$

It was historically used most often before the advent of high-resolution multipass Fabry–Pérot interferometers, presumably because Rayleigh scattering is minimal for this scattering angle. In the platelet geometry [Fig. 1(c)], the involved phonon propagates in a direction along the platelet plane and satisfies

$$\omega_3 = q_3 v = 2kv \sin\theta. \tag{3}$$

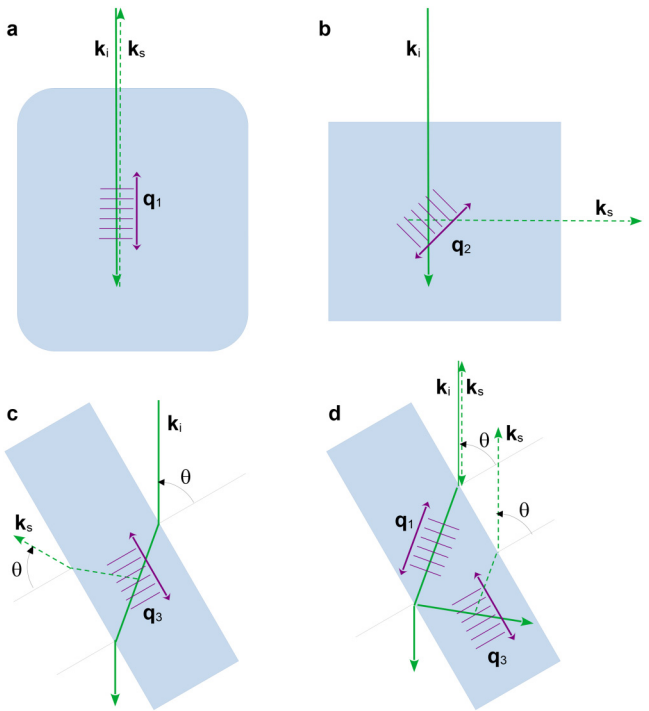

FIG. 1. BLS geometries. (a) Backscattering or 180°-scattering involving phonon $\mathbf{q}_1$ satisfying Eq. (1). (b) 90°-scattering involving phonon $\mathbf{q}_2$ satisfying Eq. (2). (c) Platelet geometry involving phonon $\mathbf{q}_3$ satisfying Eq. (3). (d) Backscattering-platelet geometry involving both phonons $\mathbf{q}_1$ and $\mathbf{q}_3$.

Note the absence of the index of refraction in the last relation but the dependence with the angle of incidence θ. Precise alignment and platelet parallelism are hence required but the velocity is directly estimated.[7]

As the above relations indicate, the determination of experimental Brillouin frequencies enables the joint estimation of the index of refraction and of the phonon velocity. It is necessary for this purpose to combine at least two phase-matching geometries providing complementary information.[8,9] Those geometries can be implemented separately in the experiment or encoded using a specific aperture in an optical microscope.[10,11] The latter solution is favored for biological samples that have to be imaged at a microscopic scale.[12,13]

In addition to the classic scattering geometries described above, Krüger *et al.*[14] identified a fourth one, which they termed RIΘA, but which we refer to as the platelet-backscattering geometry in the following [Fig. 1(d)]. In addition to the usual $\mathbf{q}_1$ backscattering phonon, it includes an internal reflection on the backside of the platelet and scattering by a phonon propagating in a direction along the platelet plane. The Brillouin shift obeys the same Eq. (3) as for the platelet geometry, as indeed the same $\mathbf{q}_3$ phonon is involved. As a note, the same relation is also valid for surface Brillouin backscattering, but v is in the latter case the velocity of a surface phonon and not a bulk phonon.[2]

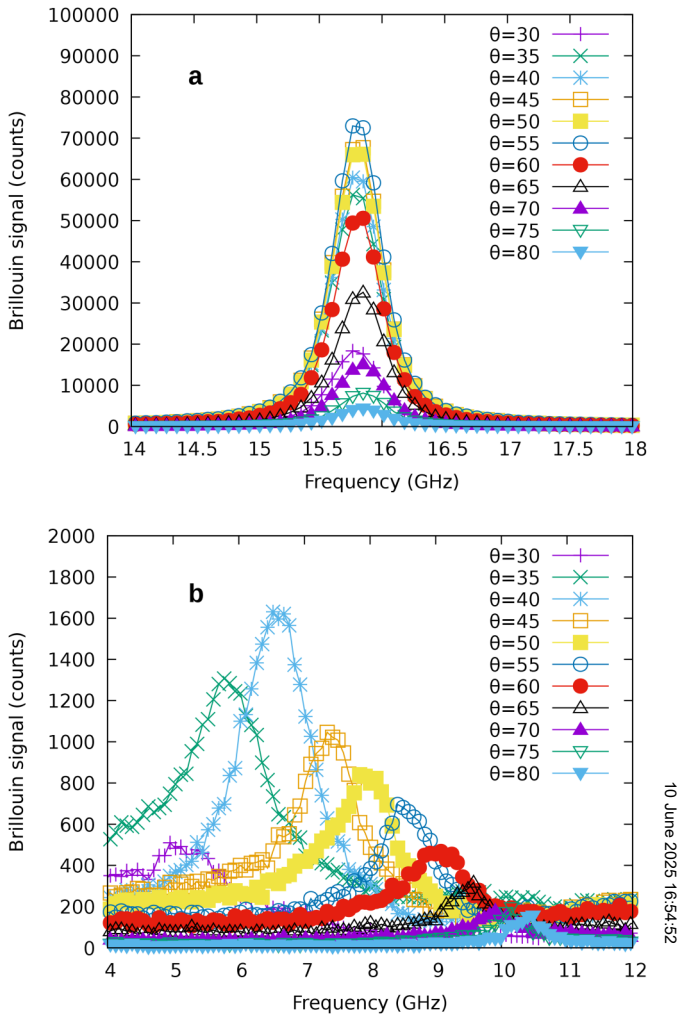

FIG. 2. Anti-Stokes part of the Brillouin spectrum for a PMMA platelet for various angles of incidence θ. (a) Primary (backscattering) and (b) secondary (RIΘA) Brillouin peaks.

In the following, we argue that when the sample assumes the shape of a transparent platelet, the secondary Brillouin signal provided by the platelet-backscattering phonon $\mathbf{q}_3$ can be used in conjunction with the primary Brillouin signal provided by the usual backscattering phonon $\mathbf{q}_1$ to estimate both optical index and phonon velocity, even in the absence of a backside reflection coating and hence without the need to alter the sample surface. Even though the secondary signal is much weaker than the primary signal, the Brillouin shift is independent of the index of refraction and its dependence on the angle of incidence provides enough diversity for improving the overall fit process. Furthermore, no special alignment procedure is required if the platelet has parallel facets.

TABLE I. Center frequency and FWHM for both primary (f_1 and Γ_1) and secondary (f_2 and Γ_2) Brillouin peaks, for the PMMA platelet.

θ (deg)	f_1 (GHz)	Γ_1 (GHz)	f_2 (GHz)	Γ_2 (GHz)
30	15.8374	0.42	5.2216	1.66
35	15.8434	0.42	5.8681	1.68
40	15.8447	0.41	6.5862	1.41
45	15.8465	0.41	7.3541	1.25
50	15.8508	0.41	7.8968	1.27
55	15.8543	0.41	8.5326	1.18
60	15.8549	0.41	8.9516	1.46
65	15.8581	0.41	9.4835	1.08
70	15.8592	0.41	9.8625	1.34
75	15.8602	0.41	10.1425	0.79
80	15.8591	0.41	10.3975	0.68

II. MEASUREMENTS

Measurements were conducted in a backscattering configuration utilizing a single longitudinal mode laser operating at a wavelength of 532 nm and an incident power of 50 mW. To achieve precise detection of bulk acoustic phonons, a six-pass Tandem Fabry–Pérot interferometer (JRS Instruments, model TFP2-HC) was employed, with a finesse of about 100. The interferometer mirror spacing was set to $d = 6$ mm for PMMA (polymethyl methacrylate) and $d = 3$ mm for fused silica and soda-lime glass. Other experimental details are as used for crystal samples.[3] In particular, the numerical aperture of the collecting lens is 0.1. Instrumental broadening is taken into account in the software used to fit Brillouin peaks. In all experiments, the scanning amplitude was maintained at 450 nm. The measured thickness of the PMMA platelet is 3.5 and 0.7 mm for the fused silica and soda-lime glass platelets.

Measurements as a function of the angle of incidence are collected in Fig. 2 for the PMMA platelet. Though the secondary and the primary peaks are shown separately, because their maximum intensities are quite different, they were both acquired at the same time for each angle of incidence. Both peaks are fitted simultaneously against the sum of two damped harmonic oscillator (DHO) functions and an exponentially decreasing background accounting for elastic Rayleigh scattering. The center frequencies f_i and the full-widths at half maximum (FWHM) Γ_i are listed in Table I for both peaks. They are next used to estimate the index of refraction and the phonon velocity. It is noted that f_1 and Γ_1 are almost independent of θ, in contrast to f_2 and Γ_2. The peak width Γ_2 actually decreases with increasing θ, suggesting an improvement in the phonon wavenumber selection inside the platelet and hence an increasing confidence in the quality of the measurement.

III. RESULTS AND DISCUSSION

The usual approach in the backscattering geometry is to fit only the primary contribution to the Brillouin spectrum (fit type A in Table II). Indeed, it can be observed in Fig. 2 that the primary peak is much stronger than the secondary peak (by a factor of 50, approximately) and the DHO function is sharper ($\Gamma_1/f_1 < \Gamma_2/f_2$). As a technical note, we use the inverse of the FWHM as a weighting function in the least-squares objective function for the Levenberg–Marquardt fit procedure, to account for individual peak quality. As a result, the fit of the central frequency is quite accurate (0.015% for the PMMA platelet in Table II). Assuming the index of refraction is known, this precision translates directly to the longitudinal phonon velocity v. This confidence arising from the quality of the measurement, however, does not exclude the possibility of a bias caused by the assumed value for n.

An alternative approach we follow here is to fit both primary and secondary contributions to the Brillouin spectrum, estimating simultaneously n and v (fit type B in Table II). As a result, the confidence in the fit is equalized over both fitted parameters.

For PMMA, the simultaneous fit leads to corrected values for both n and v compared to the usual approach. It appears the assumed value for n was off by about 1.4%, resulting in a velocity bias of 38 m/s, which is small but significantly larger than the usual

TABLE II. Parameter estimation of index of refraction n and longitudinal velocity v using the Levenberg–Marquardt fit procedure. All the spectra collected for each sample are analyzed simultaneously. For each of the three platelet samples considered, v is first fitted from the primary Brillouin signal only assuming n is known (fit type A). Then, n and v are simultaneously fitted from both primary and secondary Brillouin signals (fit type B). n, v, and θ_0 (incidence angle bias) are further simultaneously fitted from both primary and secondary Brillouin signals (fit type C). Finally, only v and θ_0 are fitted from secondary Brillouin signals (fit type D).

Platelet	Fit type	n	v (m/s)	θ_0 (deg)	rms error (GHz)
PMMA	A	1.4934[15]	2823.5 ± 0.4 (0.015%)	0	0.019
	B	1.5139 ± 0.0030 (0.20%)	2785.3 ± 5.5 (0.20%)	0	0.053
	C	1.499 ± 0.0030 (0.20%)	2812.5 ± 5.5 (0.20%)	−1.2 ± 0.2 (16%)	0.031
	D	…	2812.5 ± 7.2 (0.26%)	−1.2 ± 0.2 (21%)	0.041
Fused silica	A	1.4607[15]	5962.9 ± 0.5 (0.008%)	0	0.018
	B	1.4651 ± 0.0017 (0.11%)	5944.9 ± 6.4 (0.11%)	0	0.081
	C	1.4626 ± 0.0028 (0.19%)	5955.0 ± 11.4 (0.19%)	−0.28 ± 0.25 (92%)	0.081
	D	…	5955.0 ± 16.3 (0.27%)	−0.28 ± 0.36 (132%)	0.12
Soda-lime glass	A	1.5261[15]	5828.9 ± 0.4 (0.007%)	0	0.015
	B	1.5236 ± 0.0010 (0.07%)	5838.5 ± 3.6 (0.06%)	0	0.045
	C	1.5192 ± 0.0012 (0.08%)	5855.5 ± 4.5 (0.08%)	−0.47 ± 0.10 (21%)	0.031
	D	…	5855.5 ± 6.1 (0.10%)	−0.47 ± 0.14 (29%)	0.043

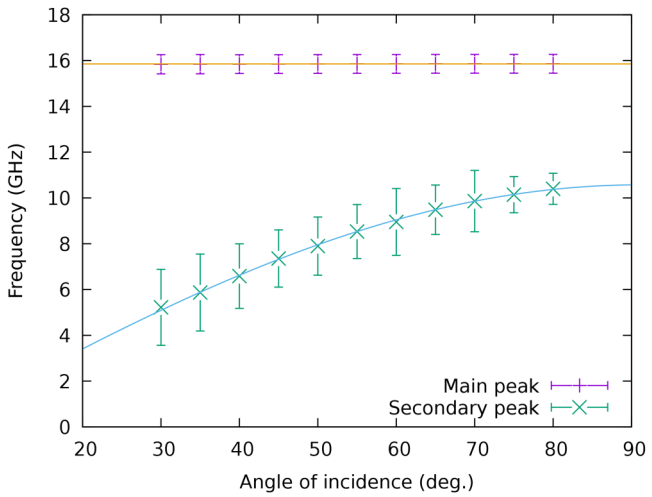

FIG. 3. Comparison of experimental and fitted Brillouin frequencies, for the PMMA platelet. The full-width at half-maximum is given as an error bar for each measured Brillouin peak.

fit confidence (0.4 m/s). The observed deviation from the standard value may result from the preparation method of PMMA. Indeed, pure poly(methyl methacrylate) homopolymer is rarely commercialized, and modified formulations contain varying amounts of other comonomers, additives, and fillers. Hence, our measurement may indicate that the measured sample was not pure PMMA, but it could also result from an experimental bias. A first source of bias could be a deviation from the condition of parallelism of the facets of the platelet, which impacts the central frequency of the secondary Brillouin peak but has no influence on the primary peak. The Appendix examines the consequence of the existence of a non-zero apex angle α. The fit deviation is linear with this angle in a first approximation and can be bounded as $\Delta\omega_3/\omega_3 < n\alpha$. As a note, a similar sensitivity analysis applies to the usual platelet scattering geometry. A second source of bias is the calibration of the incidence angle with respect to the entrance facet. This operation is performed in practice by observing the backreflection from the surface of the platelet and aligning incident and reflected laser beams thanks to a pinhole. Assuming there remains a bias θ_0, Eq. (3) changes to

$$\omega_3 = q_3 v = 2kv\sin(\theta + \theta_0). \tag{4}$$

The same backreflection check should reveal the non parallelism of the platelet, from the different reflections and in proportion to the platelet thickness. With our samples, we estimated that the parallelism bias is not significant and we, thus, decided to fit both Brillouin peaks at once, but now estimating simultaneously n, v, and θ_0 (fit type c in Table II). The fitted value of the index of refraction of PMMA in Table II is this time closer to the standard one. A comparison of experimental data and the two fitting functions (1) and (3) is shown in Fig. 3.

A fundamental question is the correlation among the fitted parameters n, v, and θ_0. Indeed, n solely appears in Eq. (1) and θ_0 only appears in Eq. (4), whereas v appears in both equations but

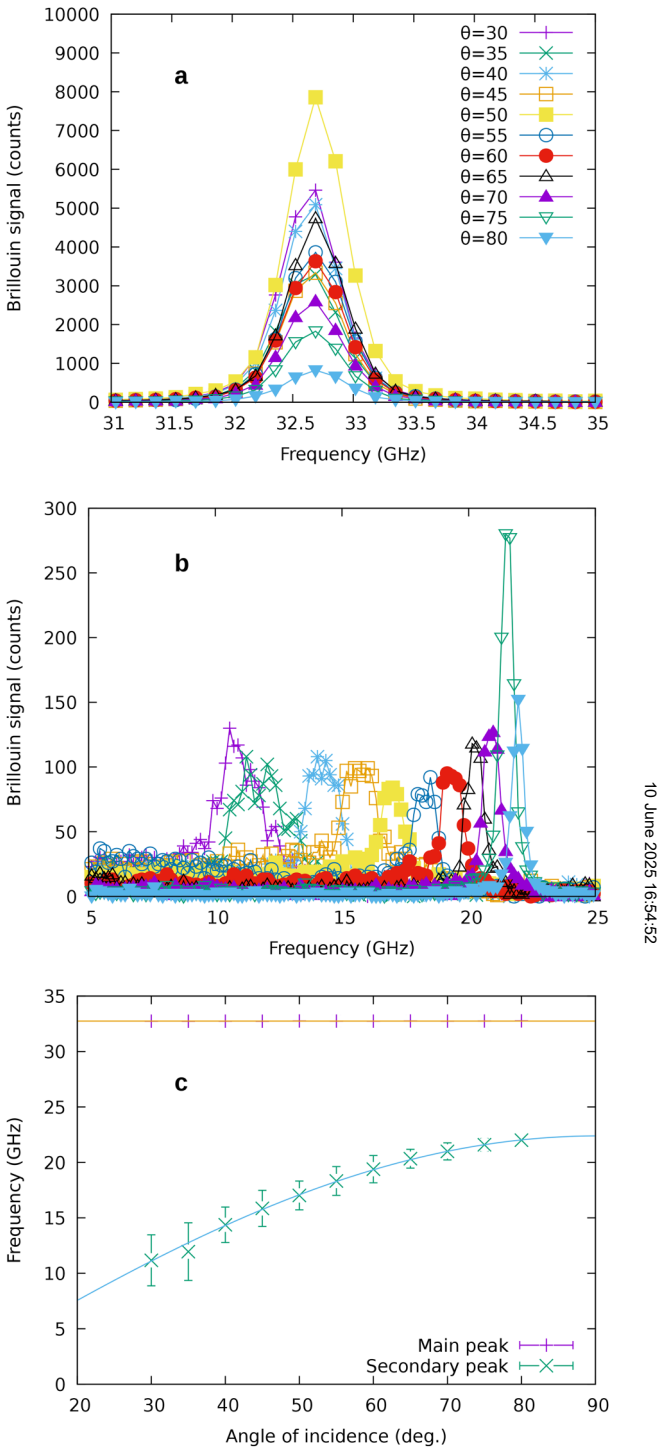

FIG. 4. Anti-Stokes part of the Brillouin spectrum for a fused silica platelet. (a) Primary and (b) secondary Brillouin peaks. (c) Comparison of experimental and fitted Brillouin frequencies. The full-width at half-maximum is given as an error bar for each measured Brillouin peak.

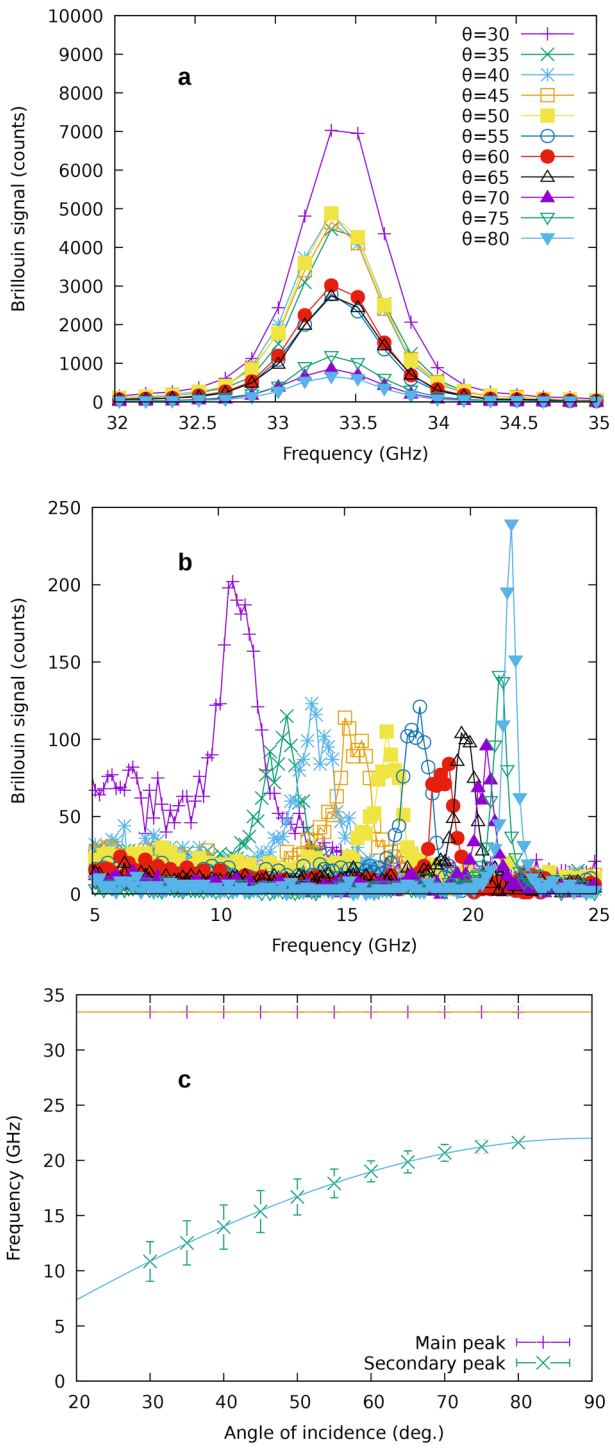

FIG. 5. Anti-Stokes part of the Brillouin spectrum for a soda-lime glass platelet. (a) Primary and (b) secondary Brillouin peaks. (c) Comparison of experimental and fitted Brillouin frequencies. The full-width at half-maximum is given as an error bar for each measured Brillouin peak.

multiplied by n in Eq. (1). As a result, it follows that in the joint estimation process the secondary Brillouin data determine the fitted values of v and θ_0, but the primary Brillouin data have no influence upon them. This property is numerically demonstrated as fit type D in Table II. It can consequently be concluded that in the joint estimation process the primary Brillouin data determine the fitted value of n.

The same measurements and fit procedures were repeated for a fused silica platelet and a soda-lime glass platelet. The measured primary and secondary Brillouin peaks for the fused silica and the soda-lime glass platelet samples are given in Figs. 4 and 5. The experimental conditions are exactly the same as for the PMMA platelet, including laser power and acquisition time. Compared with the PMMA platelet, the confidence in the results of fit type A is even stronger, but arises from the stability of measurements in the usual backscattering configuration; the possible bias in the index of refraction does not impact this confidence and cannot be revealed by primary Brillouin data alone. Considering fit type B, for the fused silica platelet, the fitted value and the assumed value for n differ by 0.3%, while the velocity differs by 18 m/s; for the soda-lime glass platelet, the fitted value and the assumed value for n differ by 0.16%, while the velocity differs by 9.6 m/s. Those corrections are indeed small, but still larger than the fit confidence. For both fit types B and C, the fitted value for n remains close to the standard value, and the fit results are similar. It appears the calibration error of the angle of incidence was smaller than in the case of the PMMA platelet and impacts less the fitting process.

In practice, the choice between fit types depends on the information available on the refractive index of the platelet. If the value is known accurately (e.g., better than 0.1% here) and can be trusted, then fit type A is best to estimate the velocity; if it is unknown or inaccurate, then fit type C gives a good estimate for both refractive index and velocity.

Only longitudinal phonons were observed in the experiments with isotropic solids reported herewith, but it should be noted that shear phonons could in principle also give another secondary Brillouin signal, as with the platelet geometry. In the general case of anisotropic solids, similarly, both primary and secondary shear Brillouin peaks could be observable, so that information regarding the shear velocities could be gained as well.

IV. CONCLUSION

Summarizing, the Brillouin spectrum for inelastic light scattering may contain two thermal phonon contributions in the platelet-backscattering geometry. The primary peak follows the usual backscattering phase-matching relation for wavevectors, but the secondary peak appearing at a lower frequency follows the platelet phase-matching relation. The resulting diversity in the dependence of the Brillouin frequency enables the precise, simultaneous estimation of the refractive index and of the longitudinal phonon velocity, and the correction of a possible calibration error of the angle of incidence. This procedure can be useful for the characterization of transparent materials whose index of refraction is not precisely known otherwise. It could also be extended to anisotropic media as a perspective. In this case, the full elastic tensor, giving the phase velocities of quasi-shear and quasi-longitudinal phonons, can be estimated by selecting a proper set of incidence

angles,[3] though the fit procedure used indeed needs the refractive indices to be known. A set of measurements performed in the platelet-backscattering geometry, by varying the incidence angle, could help to refine an initial approximate starting value for the refractive indices while simultaneously estimating the full elastic tensor.

ACKNOWLEDGMENTS

This work has been supported by the EIPHI Graduate school (Contract No. "ANR-17-EURE-0002") and by the Bourgogne-Franche-Comté Region. Support from the French RENATECH network and its FEMTO-ST technological facility is also gratefully acknowledged.

AUTHOR DECLARATIONS

Conflict of Interest

The authors have no conflicts to disclose.

Author Contributions

Fehima Ugarak: Conceptualization (equal); Data curation (lead); Investigation (lead); Software (equal); Visualization (lead); Writing – original draft (equal). **Alexis Mosset:** Resources (lead); Supervision (equal); Validation (equal); Writing – review & editing (equal). **Vincent Laude:** Conceptualization (equal); Formal analysis (lead); Methodology (lead); Software (equal); Supervision (equal); Writing – original draft (equal).

DATA AVAILABILITY

The data that support the findings of this study are openly available in Zenodo at https://doi.org/10.5281/zenodo.15109271, Ref. 16.

APPENDIX: SENSITIVITY TO THE PARALLELISM CONDITION

A platelet has by definition two parallel flat facets. If the bottom facet, on which reflection occurs, makes an angle α with respect to the top facet, then the phonon wavevector is

$$\mathbf{q}_3 = \pm 2kn\sin(\theta_i + \alpha)\begin{pmatrix}\cos\alpha\\ \sin\alpha\end{pmatrix} \tag{A1}$$

in the reference frame attached to the platelet (axis x along the platelet axis, axis y normal to the parallel faces). θ_i is the internal incidence angle satisfying $n\sin\theta_i = \sin\theta$ according to the Snell-Descartes law of refraction. Thus, an error in the parallelism of the platelet causes the phase-matching condition for the secondary peak (3) to become

$$\omega_3 = 2knv\sin(\theta_i + \alpha) = 2knv\sin\left(\sin^{-1}\left(\frac{1}{n}\sin\theta\right) + \alpha\right). \tag{A2}$$

The error made appears as if the definition of the incidence angle had been shifted by the apex angle α when measured inside the platelet. For small angle α we have

$$\omega_3 \approx 2kv\left(\sin\theta + \alpha\sqrt{n^2 - \sin^2\theta}\right) \tag{A3}$$

and the deviation is linear with α. In the first order, the frequency deviation has an upper bound

$$\Delta\omega_3/\omega_3 < n\alpha. \tag{A4}$$

Finally, both apex angle and incidence angle errors can be combined in the same formula

$$\omega_3 = 2knv\sin\left(\sin^{-1}\left(\frac{1}{n}\sin(\theta + \theta_0)\right) + \alpha\right). \tag{A5}$$

Unfortunately, both errors affect in a similar way the Brillouin frequency and we observed numerically that it is not significant to fit simultaneously both θ_0 and α. Hence, in fit type C we assumed $\alpha = 0$. An independent determination of the apex angle could be used to improve the fit formula.

REFERENCES

[1]F. Kargar and A. A. Balandin, "Advances in Brillouin–Mandelstam light-scattering spectroscopy," Nat. Photonics **15**, 720–731 (2021).
[2]G. Carlotti, "Elastic characterization of transparent and opaque films, multilayers and acoustic resonators by surface Brillouin scattering: A review," Appl. Sci. **8**, 124 (2018).
[3]F. Ugarak, J. A. Iglesias Martínez, A. Mosset, and V. Laude, "Estimation of the elastic and piezoelectric tensors of sapphire and lithium niobate from Brillouin light backscattering measurements of a single crystal sample," J. Appl. Phys. **134**, 185103 (2023).
[4]A. Polian, "Brillouin scattering at high pressure: An overview," J. Raman Spectrosc. **34**, 633–637 (2003).
[5]S. Speziale, H. Marquardt, and T. S. Duffy, "Brillouin scattering and its application in geosciences," Rev. Mineral. Geochem. **78**, 543–603 (2014).
[6]J. Sandercock, "Trends in Brillouin scattering: Studies of opaque materials, supported films, and central modes," in *Light Scattering in Solids III: Recent Results* (Springer Verlag, 2005), pp 173–206.
[7]L.-g. Liu, C.-c. Chen, C.-C. Lin, and Y.-j. Yang, "Elasticity of single-crystal aragonite by Brillouin spectroscopy," Phys. Chem. Miner. **32**, 97–102 (2005).
[8]J. Krüger, A. Marx, L. Peetz, R. Roberts, and H. G. Unruh, "Simultaneous determination of elastic and optical properties of polymers by high performance Brillouin spectroscopy using different scattering geometries," Colloid Polym. Sci. **264**, 403–414 (1986).
[9]E. Zouboulis and M. Grimsditch, "Refractive index and elastic properties of single-crystal corundum (α-Al_2O_3) up to 2100 K," J. Appl. Phys. **70**, 772–776 (1991).
[10]A. Fiore, C. Bevilacqua, and G. Scarcelli, "Direct three-dimensional measurement of refractive index via dual photon-phonon scattering," Phys. Rev. Lett. **122**, 103901 (2019).
[11]K. Elsayad, "A new angle on mapping the refractive index," Physics **12**, 27 (2019).
[12]D. Fioretto, S. Caponi, and F. Palombo, "Brillouin-Raman mapping of natural fibers with spectral moment analysis," Biomed. Opt. Express **10**, 1469–1474 (2019).
[13]F. Palombo and D. Fioretto, "Brillouin light scattering: Applications in biomedical sciences," Chem. Rev. **119**, 7833–7847 (2019).
[14]J. K. Krüger, J. Embs, J. Brierley, and R. Jiménez, "A new Brillouin scattering technique for the investigation of acoustic and opto-acoustic properties: Application to polymers," J. Phys. D: Appl. Phys. **31**, 1913 (1998).
[15]M. N. Polyanskiy, "Refractiveindex.info database of optical constants," Sci. Data **11**, 94 (2024).
[16]F. Ugarak, A. Mosset, and V. Laude, (2025) "Brillouin backscattering spectra for PMMA, fused silica, and soda lime glass," Zenodo (2025). https://doi.org/10.5281/zenodo.15109271